AUTOMATED SPECTRO-GONIOMETER: A ROBOTIC ARM FOR THE MEASUREMENT OF SNOW BI-DIRECTIONAL REFLECTANCE DISTRIBUTION FUNCTION

Thomas H. Painter, Bradley E. Paden, and Jeff Dozier

ABSTRACT

We describe the UCSB Automated Spectro-Goniometer (ASG), a two-axis robotic arm paired with a field spectroradiometer for the rapid and accurate measurement of the optical bi-directional reflectance distribution function (*BRDF*) of snow. Improvements in radiative transfer models and remote sensing algorithms for snow properties require a more accurate characterization of the angular distribution of reflectance of snow. Previous measurements of snow *BRDF* have been incomplete with respect to one or more of spectral range, spectral resolution, angular resolution and sampling, solar zenith sampling, and snow characterization. The kinematics of the ASG may be described by *Rodrigues' formula* for a 2 degree of freedom arm. We describe the forward kinematics for the ASG and then solve the inverse problem from given view angle to necessary rotation about each axis. Its two-dimensional hemispheric sampling space facilitates the measurement of spectral reflectance from snow into any direction. The ASG will usually sample a 10° hemispheric grid at a 0.5 Hz sampling rate. We will also sample the solar principal plane at 1° angular resolution at 0.5 Hz sampling rate. With a total weight of 41 kg, the ASG is easily portable by an individual via sled.

1. INTRODUCTION

Distributed snowmelt models require input and validation of snow covered area, grain size, albedo, and snow water equivalent. Estimates of all but snow water equivalent are available from optical (solar) remote sensing. Algorithms for retrieving these snow properties have been based on an unfortunate, but computationally necessary, assumption; that snow reflects spectral solar radiation isotropically. However, snow has an anisotropic reflectance distribution that is further complicated by a dependence on wavelength and grain morphology (*Warren*, 1982; *Leroux et al*, 1998). Satellites sample only a part of this spectral *BRDF* (bi-directional reflectance distribution function) that has been convolved with interactions on rough alpine terrain. Hence, the assumption of isotropic reflectance will frequently produce errors in quantitative snow property retrievals. Recent surges in computational power and data storage have enabled scientists to develop and refine quantitative retrievals by incorporating the *BRDF*. While models for snow *BRDF* abound, a comprehensive sampling of snow *BRDF* and its dependence on solar geometry, wavelength, grain size distribution, grain morphology, liquid water content, and impurities does not exist. To meet this need, we have developed an automated robotic arm for use with a high spectral resolution field spectroradiometer. In this paper, we describe the Automated Spectro-Goniometer (ASG) in terms of its constraints, kinematics and dynamics, spectral range and resolution, sampling protocols, and specifications. We begin with a definition of *BRDF* and a discussion of previous measurements of snow *BRDF*.

1.1. Bi-directional Reflectance Distribution Function

The *bi-directional reflectance distribution function* (*BRDF*) of a surface is expressed as:

$$(1) \qquad BRDF_\lambda(\theta_0,\phi_0;\theta_r,\phi_r)=\frac{L_\lambda(\theta_r,\phi_r)}{\mu_0 E_\lambda(\theta_0,\phi_0)}$$

where L_λ is spectral radiance ($Wm^{-2}sr^{-1}\mu m^{-1}$), E_λ is spectral irradiance ($Wm^{-2}\mu m^{-1}$) onto a plane normal to the beam, θ_o is zenith angle of irradiance, θ_r is the zenith angle of reflected light, ϕ_o is the azimuth angle of irradiance, ϕ_r is the azimuth angle of reflected light and μ_0 is the cosine of θ_o. *BRDF* has units of sr^{-1}. The physical concept of the *BRDF* is shown in Figure 1. Simplified, the *BRDF* describes the magnitude of reflected radiance into a direction relative to the irradiance from a given direction.

A more useful, unit-less form of the distribution is the *bi-directional reflectance factor (BRF)*:

$$(2) \qquad BRF_\lambda(\theta_0,\phi_0;\theta_r,\phi_r)=\frac{\pi\, L_\lambda(\theta_r,\phi_r)}{\mu_0 E_\lambda(\theta_0,\phi_0)}$$

Contact information for first author: Thomas H. Painter, Institute for Computational Earth System Science, University of California, Santa Barbara, CA 93106; painter@icess.ucsb.edu; phone: (805) 893-8116; fax: (425) 740-9260, URL: http://www.icess.ucsb.edu/~painter/

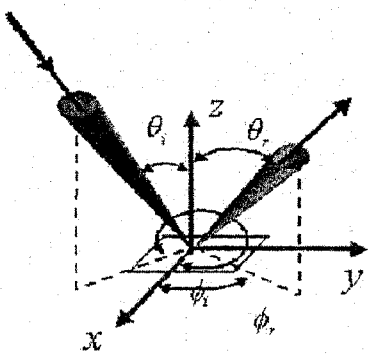

Figure 1 Bi-directional reflectance distribution.

BRF is the ratio of radiance reflected into the direction θ_r, ϕ_r to the radiance that would be reflected into any direction by a perfectly reflecting Lambertian surface. The final product of the ASG is the *BRF* for a particular surface. For simplicity, we will refer to *BRDF* and *BRF* as simply *BRDF* unless otherwise noted.

For energy balance and snowmelt modeling, the more important optical property is the spectral albedo, A_λ. It is expressed as the integral of the *BRDF* over the upper hemisphere:

$$(3) \qquad A_\lambda(\theta_0) = \int_0^{2\pi}\int_0^{\pi/2} BRDF_\lambda(\theta_0,\phi_0;\theta_r,\phi_r)\sin\theta_r\cos\theta_r\, d\theta_r\, d\phi_r$$

1.2. Previous Snow *BRDF* and *BRF* Measurements

The literature describing the *BRDF* of snow is sparse. Previous efforts to characterize the *BRDF* of snow have been limited with respect to one or more of angular resolution and range, spectral resolution and spectral range, speed of acquisition, and quantitative documentation of snow properties (*O'Brien and Munis*, 1975; *Steffen*, 1987; *Grenfell et al*, 1994). *Dozier et al* (1988) addressed deficiencies of previous experiments with greater angular sampling and resolution, greater spectral resolution, and more detailed snow characterization. However, the spectrometer they used was sensitive only to $\lambda \approx 1.0$ μm, at the shorter wavelength end of the spectral region in which the reflectance of snow is most sensitive to grain size and

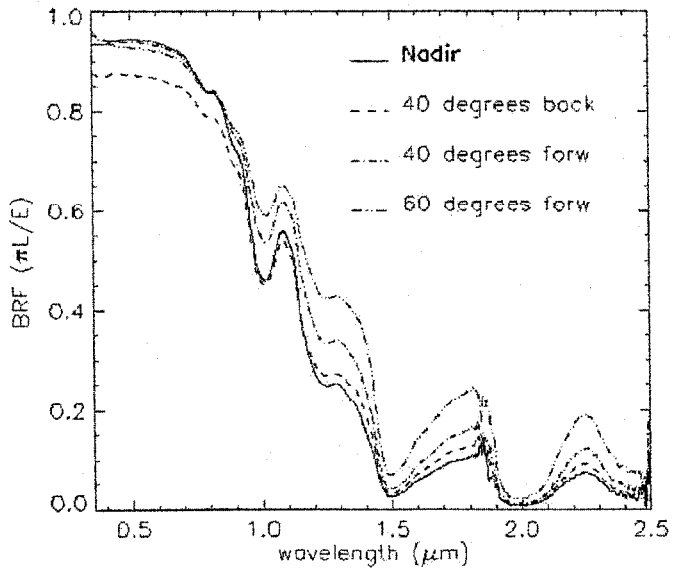

Figure 2 *BRDF* measurements, Mammoth Mountain, CA, 4/25/1999, fine grain.

dominant in controlling albedo. Recent measurements of snow *BRDF* have been accompanied by detailed quantification of grain size distribution and grain morphology (*Leroux et al*, 1998), yet only at a few discrete bands across the visible and near-infrared.

In Figure 2, we show *BRF* spectra acquired on Mammoth Mountain, CA in April 1999. These data demonstrate the anisotropy of the *BRF* of snow and the potential for error in inferring grain size and albedo from a single angle measurement. In the spectral range 900 – 1400 nm, difference between nadir views and 60° forward are up to ~ 20% absolute and ~80% relative. In the spectral range 1500 – 2500 nm, differences are up to ~20% absolute and ~100% relative. Most satellites do not acquire data with a 60° view zenith, but rough topography will frequently pose large local view zeniths where anisotropic effects are most pronounced.

2. DESCRIPTION OF THE SYSTEM

A comprehensive characterization of snow *BRDF* must address two sets of parameters, one set corresponding to instrumentation and the other corresponding to snow and atmospheric characterization. The former consists of spectral range and resolution, acquisition speed, angular range and resolution, angular accuracy, and acquisition speed (if using the Sun as an illumination source). The latter consists of the spectral ratio of diffuse to direct irradiance, grain size distribution, grain morphology and its distribution, snow liquid water content, density, and impurities. In this section, we will discuss the instrumentation set of parameters. In Section 4, we discuss the protocol of use of the ASG and the accompanying snow and atmospheric characterization.

The core of the ASG is an Analytic Spectral Devices (ASD) FR FieldSpec Field Spectroradiometer (http://www.asdi.com). Table 1 shows the specifications of the ASD-FR. Of note here are the complete spectral range (350 – 2500 nm), high spectral resolution (3 – 10 nm), and the rapid spectrum acquisition (10 spectra / s). With the rapid spectrum acquisition, we are able to access a dense grid of points on the hemisphere above the snow target with little solar movement.

The ASD-FR optic cable endpoint is attached to the end of the lower arm of the ASG. The geometry dictates that the optic cable is always pointed at the center of the base circle (discussed in Section 3). The scanning space is the hemisphere above this center. Using brushless servo motors, the optic cable endpoint may be placed at any point on the hemisphere. Hence, we have arbitrary angular range and resolution. In design and manufacture, we specified angular accuracy at $\pm 1^{\circ}$. The Pittman motors described below have 2000 counts per revolution which combined with 72 and 95 teeth worm gears easily meets the angular accuracy constraint.

3. KINEMATICS AND DYNAMICS

Given the above system description, we now analyze the kinematics of the mechanism using the terminology of *Tsai* (1999). The foreoptic mount moves in the hemisphere of constant radius about the target. As such, the mechanism functions in a space with $\lambda = 3$ degrees of freedom. The degrees of freedom for a mechanism with no passive degrees of freedom is defined by the *Grübler criterion*:

$$(4) \qquad F = \lambda\left(n - j - 1\right) + \sum_{i} F_i$$

Analytical Spectral Devices FR Spectroradiometer	Specifications
Spectral Range	350 – 2500 nm
Spectral Resolution	3 nm (350-1000 nm), 10 nm (1000-2500 nm)
Spectrum Sampling Rate	10 spectra / s
Weight	7 kg + 2.2 kg battery = 9.2 kg
Optic Cable Length	2.5 m
Foreoptics	1°, 4°, 8°

Table 1 Specifications for the Analytical Spectral Devices FR FieldSpec Spectroradiometer.

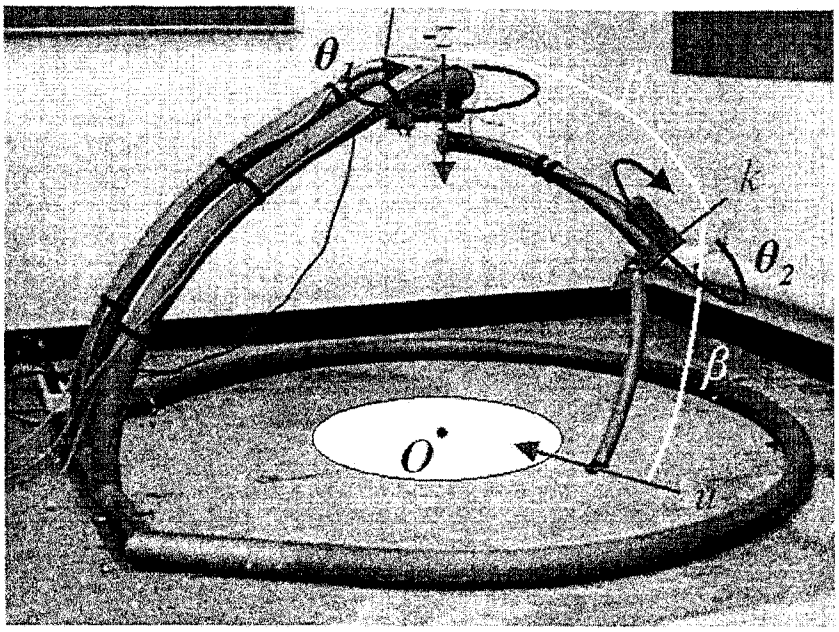

Figure 3 Geometry of ASG. Snow target is centered at $\boldsymbol{O}$, $\boldsymbol{u}$ is the view vector, β is the arm angular arc, -z (vertical) is the upper arm axis, $\boldsymbol{k}$ is the lower arm axis, θ_1 is the rotation about $-\boldsymbol{z}$, and θ_2 is the rotation about $\boldsymbol{k}$. $\boldsymbol{u}$, $\boldsymbol{k}$, and $-\boldsymbol{z}$ all intersect at $\boldsymbol{O}$.

where n is the number of links in a mechanism (including the fixed link), j is the number of joints in a mechanism (assuming that all the joints are binary), and f_i is the degrees of relative motion permitted by joint i. For the ASG, $n = 3 = 2$ arms + 1 frame, $j = 2 =$ shoulder + elbow, and $\Sigma(f_i) = 1 + 1$, and by the *Grübler criterion*, $F = 3(3 - 2 - 1) + (1+1) = 2$. Therefore, the ASG is a 2 DOF mechanism.

The kinematics of the ASG can be described with *Rodrigues' formula* (*Tsai*, 1999) for a spherical displacement of a rigid body. The protocol for use of the ASG is determined by a prescribed set, U, of viewing angles or view vectors $\hat{u}$. Hence, we must solve the inverse kinematics problem: given $\hat{u}$, find θ_1, θ_2. Except at full reach and full retraction of the ASG arms, there are two solutions to the inverse kinematics problem.

All joint rotations are about axes that pass through the center of the hemisphere that lies above the target. A 3x3 matrix $\boldsymbol{R}$ is a rotation matrix if:

a) $\boldsymbol{R}^T\boldsymbol{R} = \boldsymbol{I}$

b) $\det(\boldsymbol{R}) = 1$

where $\boldsymbol{I}$ is the identity matrix. All rotation matrices have an axis k for which

a) $\boldsymbol{R}k = k$

b) $k^T\boldsymbol{R} = k$

c) *and* $||k||=1$.

If k is an axis of $\boldsymbol{R}$ then

$$(5) \qquad R = (1-\cos\theta)kk^T + \cos\theta\, I + \sin\theta\,[kx]$$

where

$$[kx] \equiv \begin{bmatrix} 0 & -k_3 & k_2 \\ k_3 & 0 & -k_1 \\ -k_2 & k_1 & 0 \end{bmatrix}$$

and θ is the angle of rotation about k. Equation (5) is *Rodrigues' formula.*

The orientation of the spectrometer foreoptic is $-z$ initially. When the ASG elbow is rotated θ_2 the new orientation of the foreoptic is

$$R_k(\theta_2)(-z)$$

where

$$R_k(\theta_2)$$

is the rotation about k by θ_2. When we rotate by θ_1 about z, the orientation becomes

$$u = R_z(\theta_1)R_k(\theta_2)(-z) \tag{6}$$

where the rotation matrices can be computed from *Rodrigues' formula.*

We must now solve this equation for θ_1 and θ_2 given $\hat{u}$. Multiply (6) on the left by z^T to get

$$z^T u = z^T R_z(\theta_1)R_k(\theta_2)(-z) \tag{7}$$

and

$$z^T u = z^T R_k(\theta_2)(-z) \tag{8}$$

which can be solved for θ_2. From the figure,

$$k = \begin{pmatrix} \sin\beta \\ 0 \\ \cos\beta \end{pmatrix}$$

Substituting k into equation (5) gives:

$$\begin{aligned} R_k(\theta_2)(-z) &= -\left[(I-\cos\theta_2)kk^T z + \cos\theta_2 z + \sin\theta_2 kxz\right] \\ &= -\left[(1-\cos\theta_2)\begin{pmatrix}\sin\beta\\0\\\cos\beta\end{pmatrix}\cos\beta + \begin{pmatrix}0\\0\\\cos\theta_2\end{pmatrix} + \sin\theta_2\begin{pmatrix}0\\-\sin\beta\\0\end{pmatrix}\right] \\ &= (\cos\theta_2 - 1)\begin{pmatrix}\sin\beta\cos\beta\\0\\\cos^2\beta\end{pmatrix} - \begin{pmatrix}0\\0\\\cos\theta_2\end{pmatrix} - \begin{pmatrix}0\\\sin\theta_2\sin\beta\\0\end{pmatrix} \end{aligned} \tag{9}$$

Combining (8) and (9) gives

$$u_z = \cos\theta_2\left(\cos^2\beta - 1\right) - \cos^2\beta \tag{10}$$

$$\theta_2 = \cos^{-1}\left(\frac{u_z + \cos^2\beta}{\left(\cos^2\beta - 1\right)}\right) \tag{11}$$

where $u_z = z^T u$.

Given θ_2, we now solve for θ_1. We define w as

$$w = R_k(\theta_2)(-z)$$

and solve

$$u = R_z(\theta_1)w$$

$$(12) \quad \Rightarrow \begin{bmatrix} u_x \\ u_y \\ u_z \end{bmatrix} = \begin{bmatrix} \cos\theta_1 & -\sin\theta_1 & 0 \\ \sin\theta_1 & \cos\theta_1 & 0 \\ 0 & 0 & 1 \end{bmatrix} \begin{bmatrix} w_x \\ w_y \\ w_z \end{bmatrix}$$

$$\Rightarrow \begin{bmatrix} u_x \\ u_y \end{bmatrix} = \begin{bmatrix} \cos\theta_1 & -\sin\theta_1 \\ \sin\theta_1 & \cos\theta_1 \end{bmatrix} \begin{bmatrix} w_x \\ w_y \end{bmatrix}$$

We define α and r as follows:

$$\alpha \equiv a\tan_2\left(\frac{w_y}{w_x}\right)$$

$$r \equiv \sqrt{w_x^2 + w_y^2}$$

so that

$$w_x = r\cos\alpha$$

$$w_y = r\sin\alpha$$

Combining these definitions with (12) yields

$$\begin{bmatrix} u_x \\ u_y \end{bmatrix} = \begin{bmatrix} \cos\theta_1 & -\sin\theta_1 \\ \sin\theta_1 & \cos\theta_1 \end{bmatrix} \begin{bmatrix} r\cos\alpha \\ r\sin\alpha \end{bmatrix}$$

$$= \begin{bmatrix} r\cos\theta_1\cos\alpha - r\cos\theta_1\sin\alpha \\ r\sin\theta_1\cos\alpha + r\cos\theta_1\sin\alpha \end{bmatrix}$$

$$= r\begin{bmatrix} \cos(\theta_1 + \alpha) \\ \sin(\theta_1 + \alpha) \end{bmatrix}$$

$$\Rightarrow \quad (\theta_1 + \alpha) = a\tan_2\left(\frac{u_y}{u_x}\right)$$

$$(13) \quad \theta_1 = a\tan_2\left(\frac{u_y}{u_x}\right) - \alpha.$$

4. CONTROL

The summary of the specifications of the ASG appears in Table 2. Rotation about each axis of the ASG is driven by a Pittman 3400 Series brushless servo motor. We control the motors with a combination of Advanced Motion Control B12A6 amplifiers and a Galil Motion Control DMC-2400 motor controller. The integrated system draws 110V power. An autonomous laptop drives the motor controller via USB and interfaces via RS-232 with a laptop integrated in the ASD-FR spectroradiometer. The ASD-FR runs in automatic regular acquisition and sends a pulse to the serial port upon completion of spectrum sampling. This pulse then initiates a discrete motion of the ASG arm to the next point in the sampling grid.

The ASD-FR can sample automatically at a 1 s interval. However, we accommodate ASG arm movement (~600 ms for 15° rotation) and vibration settling by running the ASD-FR at a 2 s (0.5 Hz) interval. We will use three fundamental sampling protocols; hemisphere at 10° zenith and azimuth sampling, hemisphere at 15° zenith and azimuth sampling, and 1° zenith sampling in the solar principal plane. We show these sampling grids in Figure 4. The respective sampling times for these protocols are 5:40 (mm:ss), 2:36, and 5:42. Figure 5 shows that in the winter and spring months, a 6 minute sampling interval results in solar geometry change comparable to the 1° angular accuracy specification for the ASG. Hence, changes in solar geometry should have negligible impact on the *BRDF* results. During the summer months the changes in solar geometry are more pronounced at mid-day. However, the associated solar

Automated Spectro-Goniometer	
Angular Resolution	Arbitrary
Angular Range	Full Hemisphere
Angular Accuracy	1°
Degrees of Freedom	2
Motors	Pittman 3400 Series Brushless Servo Motors
Amplifiers	Advanced Motion Control B12A6 Trapezoidal
Motor Controller	Galil DMC-2400
ASG Hemisphere Radius	0.65 m
Total Weight	41 kg

Table 2 Specifications for the Automated Spectro-Goniometer (ASG).

zenith at these times results in a less pronounced *BRDF*. Nonetheless, we will move to the 15° sampling grid to minimize these effects.

The ASG will lie in a north-south orientation for each sample. Its north-south line is represented by that which bisects the frame symmetrically. We then initiate sampling by determining the solar azimuth angle. A front-end for the motion control software on the autonomous laptop calls subroutines for solar ephemeris (given input date, time, and geographic location) and for the axis rotations (Figure 6). The solar ephemeris subroutines (FORTRAN77) derive from the Naval Research Laboratory ftp site and we modified them with FORTRAN90 calling functions. We coded the inversion algorithms (Section 3) for motor rotations in FORTRAN90. The ASG collects spectra of a near-perfect reflecting white panel for a measurement of E/π. The ASG arm then unfolds to full extension and rotates about $-z$ until u is in the solar principal plane. A complete sampling then follows. The sampling path fixes view zenith angle and passes through all view azimuth angles, steps to the next smaller view zenith and repeats through to the nadir shot.

The foreoptic mount at the end of the lower arm can accommodate any of the standard ASD foreoptics. We will primarily use the 1° field-of-view foreoptic. The narrow field of view limits the snow heterogeneity sampled and increases the angular resolution of *BRDF* sampling. This is important because we will perform detailed snow characterization. We will also use 4° and 8° field-of-view foreoptics for sampling coarse snow and to evaluate the impacts of decreased angular resolution when measuring *BRDF*.

5. COMPUTATION OF BRDF AND BRF

Measuring *BRDF* and *BRF* with the ASD-FR consists of sampling spectra from a calibrated, near-perfectly reflecting Spectralon panel and sampling spectra from the snow target. When scaled by the calibration coefficients for the Spectralon panel, $C_{Spectralon}$, the ratio of snow surface digital numbers to Spectralon panel digital numbers produces the *BRF* (equation 14). Scaling by $1/\pi$ gives the *BRDF* (equation 15).

$$(14) \quad BRF(\theta_0,\phi_0;\theta_r,\phi_r) = C_{spectralon}\left(\frac{DN_\lambda(\theta_r,\phi_r)}{DN_{\lambda,Spectralon}(nadir)}\right)$$

$$(15) \quad BRDF(\theta_0,\phi_0;\theta_r,\phi_r) = \frac{1}{\pi}C_{spectralon}\left(\frac{DN_\lambda(\theta_r,\phi_r)}{DN_{\lambda,Spectralon}(nadir)}\right)$$

6. SNOW CHARACTERIZATION

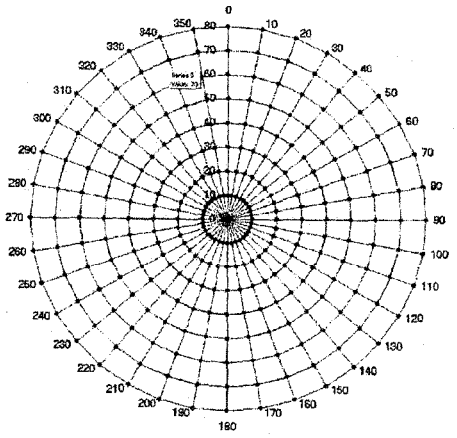

Figure 4a Sampling grid for 10° angular resolution. Points marked with '•' indicate spectral measurements. In these polar plots, radial distance represents zenith angle and angular distance from '0' represents azimuth angle. The solar principal plane corresponds to the 0-180 line with 0 toward the Sun.

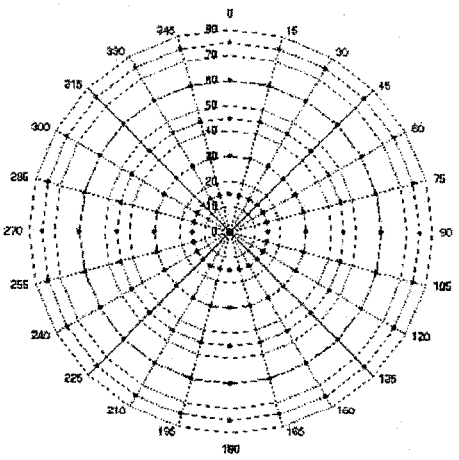

Figure 4b Sampling grid for 15° angular resolution.

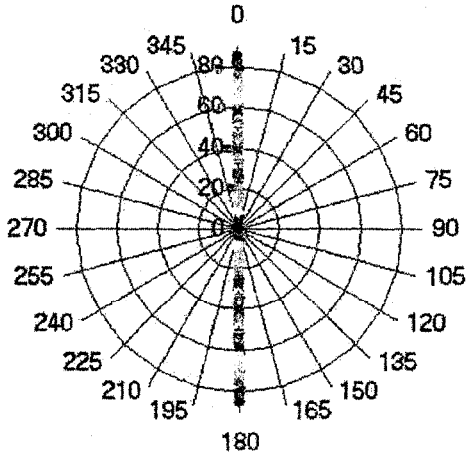

Figure 4c Sampling grid for 1° angular resolution on solar principal plane.

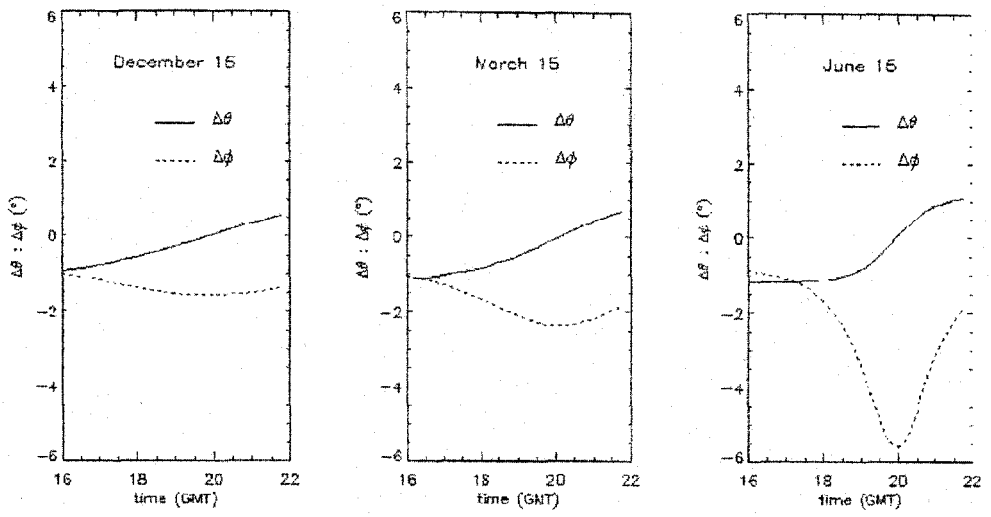

Figure 5 Change in solar geometry over a 6 minute sampling period for December 15, March 15, and June 15.

With each snow *BRDF* sampling, we will characterize the snow properties. These snow properties consist of grain size distribution, grain morphology, density, and liquid water content. We will determine grain size distribution with a combination of stereological techniques (*Davis et al*, 1985) and stratified sifting. Quantification of grain morphology will come from a digital image analysis method (*Lesaffre et al*, 1998). We will sample density stratigraphically and liquid water content with the Denoth dielectric meter (*University of Innsbruck*).

7. CONCLUSIONS

Continued development of quantitative optical remote sensing algorithms for snow properties requires knowledge of the angular distribution of reflected solar radiation from the snow surface. The Automated Spectro-Goniometer (ASG) is a 2 degree of freedom, 2-axis, robotic arm for the characterization of the bi-directional reflectance distribution function (*BRDF*) of snow. The ASG uses an Analytical Spectral Devices

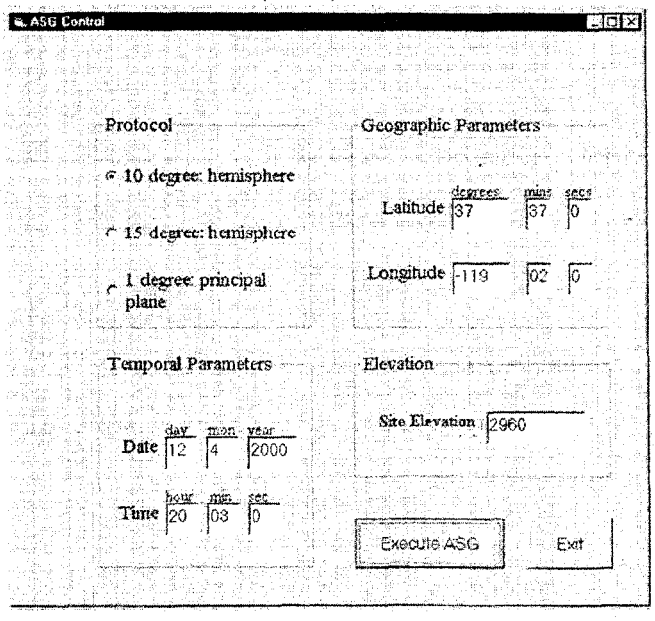

Figure 6 Control interface for Automated Spectro-Goniometer. The user specifices the protocol, site geographic parameters, the date and time, and the site elevation if solar zenith angles are > 80o. The interface serves these data to subroutines for solar ephemeris and motion control.

FR field spectroradiometer to sample reflectance spectra covering the solar spectrum at ≤ 10 nm spectral resolution. The kinematics and dynamics of the robotic arm place the spectroradiometer fore-optic at any point on the hemisphere of radius 0.65 m in order to sample the distribution of reflected solar spectra. The displacement of the robotic arm may be described by *Rodrigues' formula*. We invert *Rodrigues' formula* for the necessary rotations about both axes to describe the positions of the view vectors. A laptop coupled with a Galil DMC-2400 motor controller drives motion control. We will use three standard sampling protocols: 10° angular resolution over the hemisphere, 15° angular resolution over the hemisphere, and 1° angular resolution in the solar principal plane. Sampling at 0.5 Hz (1 point / 2 s), these protocols translate to total sampling times of 5:40 (mm:ss), 2:36, and 5:42. Over these periods, solar geometry change is minimal. We will begin sampling with the ASG in spring, 2000. The scale of the ASG permits application to other smooth surfaces such as desert, soil, tundra, and pavement.

8. ACKNOWLEDGMENTS

This work has been sponsored by the NASA IDS 'Hydrology, Hydrochemical Modeling, and Remote Sensing in Seasonally Snow-Covered Alpine Drainage Basins'. We thank Mark Shier and Hamid Baheri for engineering expertise, and Michael Colee, Bill O'Hirok, James Wilson, and Paul Ricchiazzi for discussions, suggestions, and for imparting soldering expertise to the lead author. Rincon Engineering of Carpinteria, CA machined most of the components of the ASG.

9. REFERENCES

Davis, R. E., J. Dozier, and R. Perla (1985), Measurement of snow grain properties, in *Seasonal snowcovers: physics, chemistry, hydrology*, edited by H. G. Jones and W. J. Orville-Thomas, NATO ASI Series C: Mathematical and Physical Sciences, vol. 211, pp. 53-74, D. Reidel, Dordrecht.

Dozier, J., R.E. Davis, A.T.C. Chang, and K. Brown (1988), The spectral bi-directional reflectance of snow, *Proceedings of the 4th International Colloquium on Spectral Signatures of Objects in Remote Sensing*, Aussois, France, 87-92.

Grenfell, T. C., S. G. Warren, and P. C. Mullen (1994), Reflection of solar radiation by the Antarctic snow surface at ultraviolet, visible, and near-infrared wavelengths, *Journal of Geophysical Research* 99(D9):18,669-18,684.

Leroux, C., J.-L. Deuze, P. Goloub, C. Sergent, and M. Fily (1998), Ground measurements of the polarized bi-directional reflectance of snow in the near-infrared spectral domain: Comparisons with model results, *Journal of Geophysical Research-Atmospheres* 103(ND16):19721-19731.

O'Brien, H.W. and R.W. Munis (1975), Red and near-infrared spectral reflectance of snow, *Research Report 332, U.S. Army Cold Regions Research and Engineering Laboratory*, 18 pp.

Steffen, K. (1987), Bidirectional reflectance of snow at 500-600 nm, in *Large Scale Effects of Seasonal Snow Cover*, B.E. Goodison, R.G. Barry, and J. Dozier, eds., IAHS Publication 166, 415-420.

Tsai, L.-W. (1999), Robot Analysis: The Mechanics of Serial and Parallel Manipulators, Wiley-Interscience, John Wiley & Sons, Inc., New York.

Warren, S. G. (1982), Optical Properties of Snow, *Rev. Geophys. Space Phys.* 20: 67-89.